Site-Directed Mutagenesis of Rubredoxin Reveals the Molecular Basis of Its Electron Transfer Properties

Rainer Kümmerle,[‡] Huayun Zhuang-Jackson,[§] Jacques Gaillard,[‡] and Jean-Marc Moulis*[,§]

CEA, Département de Recherche Fondamentale sur la Matière Condensée, SCIB/SCPM, and CEA, Département de Biologie Moléculaire et Structurale, Laboratoire Métalloprotéines, 17 Rue des Martyrs, 38054 Grenoble Cedex 9, France

Received July 7, 1997; Revised Manuscript Received October 8, 1997[⊗]

ABSTRACT: Rubredoxins contain a single non-heme iron atom coordinated by four cysteines. This iron is redox active and confers a role to these proteins in electron transfer chains. The structural features responsible for setting the values of the reduction potential and of the electron self-exchange rate constant have been probed by site-directed mutagenesis. Replacements of the highly conserved residues in positions 8, 10, and 11 (valine, glycine, and tyrosine, respectively) all lead to shifts of the reduction potential, up to 75 mV. These cannot be explained by simple considerations about the physicochemical properties of the substituting side chains but rather indicate that the value of the reduction potential is finely tuned by a variety of interactions. In contrast, the electron self exchange rate constant measured by nuclear magnetic resonance does not vary much, except when a charged residue is included in position 8 or 10, at the surface of the protein closest to the iron atom. Analysis of the data with a model for electrostatic interactions, including both monopolar and dipolar terms, indicates that the presence of a charge in this region not only increases the repulsion between molecules but also affects the electron transfer efficiency of the bimolecular complexes formed. The studies presented constitute a first step toward probing the structural elements modulating the reactivity of the FeS_4 unit in a protein and defining the electron transfer active site(s) of rubredoxin.

Biological transfers are formally redox or acid−base in character. Among the former, long-range electron transfer, as in electron transfer chains, plays a central role in many important cellular processes, energy-transducing reactions being prominent among them. The applicability of the electron transfer theory, established for small molecules (*1*), to biological systems is now widely accepted (*2*, *3*). The electron transfer rate depends on three parameters: electronic coupling, reorganization energy and free energy of reaction, which are characteristic of the considered system (*1*). In the very frequent case of electron transfer between proteins containing redox-active metals, the free energy of the reaction ($\Delta G°$) is directly related to the difference of the reduction potentials of the partners ($\Delta E°$) through the $\Delta G° = -nF\Delta E°$ equation, where n is the number of electrons involved and F is the Faraday constant. It is thus of primary interest to precisely assess which features tune the values of reduction potentials in redox metalloproteins as they are of fundamental importance for their function. Equally important are accurate measurements of the rates of electron transfer reactions, and their dependence on different environmental factors, as they are needed to evaluate which features determine the electron transfer efficiency.

The most immediate way a protein can modulate the electron affinity of a metal center is through the composition and number of the ligands, as exemplified by molecular variants of cytochrome *c* (*4*). However, there is plenty of evidence showing that metalloproteins sharing the same coordination sphere around the same metal (or cluster of metals) can span a very wide range of reduction potentials. This is for instance the case of the cytochrome *c* family of proteins (*5*). Thus, the tuning of the reduction potentials by the proteins involves not only the ligand field around the metal(s) but also less direct effects that contribute to the overall electrostatic potential around the metal center and determine its electron exchange properties. Among the relevant structural features considered are the hydrophobicity of the metal environment (*6*, *7*), the number of hydrogen bonds to the metal center (*8*), its solvent exposure (*5*), or the total charge of the protein molecule (*9*). Attempts at integrating the information derived from structural data to solve the Poisson−Boltzmann equation of the system have been reported (*10*−*12*). All the abovementioned properties should participate in setting the value of the reduction potential for a given family of proteins, but establishing if one, or a few, of them dominates still relies on experimental work.

The electron transfer proteins belonging to the class of the iron-sulfur proteins share an active site containing one or several (two to four) iron ion(s) in a tetrahedral coordination of sulfurs as an elemental building block. Despite the common FeS_4 geometric pattern, the iron−sulfur proteins whose function is electron transfer (they are named rubredoxins and ferredoxins) cover a range of reduction potentials (−650 to +450 mV), almost as wide as that of all biological reactions. It has been shown that ligand exchange around the iron ion can shift the value of the reduction potential (*13*−*16*), but such drastic structural changes do not always result in very large shifts (*17*−*19*). Additional effects, such as those listed above, are of importance (*8*), but their relative contributions remain to be established in most cases.

* Address correspondence to this author at CEA/Grenoble, DBMS-MEP, 17 Rue des Martyrs, 38054 Grenoble Cedex 9, France. Tel.: 33 47 688 5623. Fax: 33 47 688 5872. E-mail: moulis@ebron.ceng.cea.fr.
[†] Département de Recherche Fondamentale sur la Matière Condensée.
[§] Laboratoire Métalloprotéines.
[⊗] Abstract published in *Advance ACS Abstracts,* November 15, 1997.

S0006-2960(97)01636-X CCC: $14.00

Similarly, the value of the electron self exchange (ese)[1] constant gives an indication about the reactivity of a molecule as electron transfer agent. It can also be used to predict the rate constant for electron transfer between redox partners through the "cross-relation" (*1*).

Rubredoxin is an ideally suited protein to systematically investigate the various features tuning the reduction potential and the electron transfer properties of the FeS_4 unit. This is the only redox active center present in these proteins and several rubredoxins are structurally characterized with exceptional precision (*20*, *21*).[2] The present work reports on site-directed mutagenesis experiments of *Clostridium pasteurianum* rubredoxin to determine the salient features setting the value of the reduction potential and of the ese rate constant for this model protein.

MATERIALS AND METHODS

The production (*22*) and purification (*23*) of recombinant *C. pasteurianum* rubredoxin were already described. Protein concentrations were determined by UV−visible spectrophotometry using[3] $\epsilon_{490nm} = 6600\ M^{-1}\ cm^{-1}$, in agreement with recently published values (*24*), or $\epsilon_{750nm} = 260\ M^{-1}\ cm^{-1}$. The similarities in the spectra of the different variants, including the A_{490}/A_{280} ratios, led us to consider that the extinction coefficients were the same for all molecular forms used in this work.

Site-Directed Mutagenesis of Rubredoxin

Molecular variants were generated by an established method (*13*). Plasmid pTRD1 containing the gene encoding rubredoxin (*22*) was subjected to mutagenesis using the 5′aaatatatccacatTctgtacatgtatac oligonucleotide (the upper case letter locates the site of the change) to get the V8E form.

The other molecular variants were generated from plasmid pTRD3 in which the coding sequence of the rubredoxin gene was cloned into *Nde*I−*Hin*dIII cleaved pT7-7 (*25*). The mutagenic oligonucleotides used are shown below.

5′cgggattataaatatat(G,T)cacatactgtac for G10(A,E)

5′cgggattataaata(A,C,G)atccacatactg for Y11(F,S,C)

5′cgggattataaatat(C,G,T)tccacatactg for Y11(D,H,N)

Reduction Potential Measurements

Redox titrations were carried out under strictly anaerobic conditions (*26*). The potential was measured between the platinum and the Ag/AgCl reference of a combined electrode (Solea model XM850, Villeurbanne, France) and the UV−visible spectra were recorded with a Hewlett-Packard 8453 spectrophotometer. The reactions contained 100−200 μM rubredoxin in potassium phosphate buffer 50 mM, pH 7.0, with 5 μM each of safranine T, thionin, and indigo carmin as mediators. The absorbance at 458 nm, at which wavelength these mediators do not interfere, was used to analyze the data as described (*26*). Potentials were calculated versus the normal hydrogen electrode, using a potential of 197 mV for the Ag/AgCl (saturated KCl) electrode.

The setup for the classical electrochemical three-electrode design implemented in this work is an extension of previous devices (*27*, *28*). Electrochemical experiments were carried out in an EG&G-PAR (Princeton, NJ) microcell (model K0264) connected to a model 263 potentiostat controled with the 270/250 software. The three-electrode design included a platinum wire counter electrode, a saturated Ag/AgCl reference electrode and a glassy carbon working milli-electrode, all from EG&G. Prior to use, the 2.2 mm diameter carbon disk was extensively polished with Al_2O_3 and sonicated for 15 s, and 0.5 μL of a 20 mM neomycine (Sigma) solution in water was deposited on the surface of the electrode as promoter. About 1 μL of the rubredoxin solution was then added and the tip of the working electrode was wrapped into Spectra-Por 3 dialysis tubing (Spectrum) held around the electrode body by an O-ring. This design allowed us to use a minimal amount of material for each experiment. The electric contact with the other electrodes was made by dipping the three electrodes in ca. 1 mL of the buffer solution.

Table 1: Iron−Protein Interaction Parameters Used in Molecular Dynamics Simulations[a]

	r (Å)	force constant
Fe−S	2.26	120 kcal/(mol Å)
C−S	1.81	226 kcal/(mol Å)
	angle (deg)	force constant
C_β−S−Fe	105	45 kcal/(mol Å^2)
C−C−S	112.5	50 kcal/(mol Å^2)
S−Fe−S	109	20 kcal/(mol Å^2)
		partial charges
Fe		−0.05
S		−0.2
C_β		−0.04
C_α		0.05

[a] All improper angles were set to 0 with vanishingly small force constants.

Molecular Dynamics Simulations

The simulations used a recently determined crystallographic model for *C. pasteurianum* rubredoxin as a basis (*21*) and were carried out with CHARMm22, using the parameters for protein atoms taken from the all-atom sets (Molecular Simulations Inc., Burlington, MA). The iron center (ferrous ion) was modeled as bound to its cysteine ligands with the parameters listed in Table 1. For molecular variants G10E, V8E, and Y11N, the residue was changed using the MUTATE function implemented in Quanta. The protein was first solvated, after removing the crystallographically located water molecules, by a 8 Å-thick shell of water molecules modeled with the TIP3 potential. The system was minimized by rounds of Adopted Basis Newton Raphson cycles until convergence. Molecular dynamics simulations were started by heating the system (protein and solvent) to 300 K for 3 ps with a time step of 1 fs. Hydrogen atoms were held with SHAKE. Equilibration at this temperature was carried out for 30 ps and the system evolved for an additional 100 ps, collecting data every 0.5 ps (200 configurations). Under these conditions, the potential energy function remained constant after ca. 20 ps of simulation.

[1] Abbreviations: ese, electron self-exchange; NHE, normal hydrogen electrode; EPR, electron paramagnetic resonance; SWV, square wave voltammetry.

[2] Z. Dauter, K. S. Wilson, L. C. Sieker, J. Meyer, and J.-M. Moulis, unpublished results.

[3] J. Meyer, unpublished results.

For dipole calculations, the missing C-terminal glutamic acid in the crystallographic model was added using the protein-design module of Quanta.

Measurements of the Electron Transfer Rate Constants

The experimental setup was implemented as previously described (*29*). The ese rate constant is most precisely measured by studying the NMR lines assigned to the δCH_3 protons of Ile33, at ca. −1.2 ppm for oxidized and −1.1 ppm for reduced rubredoxin. Experiments were carried out with ca. 1:1 mixtures of oxidized and reduced protein, as determined with UV−visible spectroscopy and checked on the NMR spectra.

Theory. The Bloch equations (*30*) describe the return to equilibrium of the bulk magnetization after a perturbation. If chemical exchange occurs during the process, the time evolution of magnetization is a function of the exchange rate (*31*−*33*). Practical expressions depending on the relative values of the exchange rate and the NMR parameters have been recently summarized (*29*). Considering the following reaction of interest here,

$$Rd_{ox} + Rd_{red} \Leftrightarrow Rd_{red} + Rd_{ox},$$

the line shape of the NMR signals varies according to (*33*)

$$\upsilon(\nu) = C\left\{P\left[1 + \left(\frac{p_{red}}{T_{2ox}} + \frac{p_{ox}}{T_{2red}}\right)\right] + QR\right\}/(P^2 + R^2) \quad (1)$$

with

$$P = \tau\left\{\frac{1}{T_{2ox}T_{2red}} - 4\pi^2\Delta\nu^2 + \pi^2\delta\nu^2\right\} + \frac{p_{ox}}{T_{2ox}} + \frac{p_{red}}{T_{2red}}$$

$$Q = \tau\{2\pi\,\Delta\nu - \pi\,\delta\nu\,(p_{ox} - p_{red})\}$$

$$R = 2\pi\Delta\nu\left\{1 + \tau\left(\frac{1}{T_{2ox}} + \frac{1}{T_{2red}}\right)\right\} + \pi\delta\nu\tau\left(\frac{1}{T_{2red}} + \frac{1}{T_{2ox}}\right) + \pi\delta\nu(p_{ox} - p_{red})$$

$$\delta\nu = \nu_{ox} - \nu_{red}$$

$$\Delta\nu = \frac{\nu_{ox} + \nu_{red}}{2} - \nu$$

$$\tau = \frac{p_{ox}}{k_{ox}} = \frac{p_{red}}{k_{red}} = \frac{\tau_{ox}\,\tau_{red}}{\tau_{ox} + \tau_{red}}$$

$$k' = k_{ox} + k_{red}$$

$$k_{ese} = \frac{k'}{[Rd]} = \frac{k_{ox}}{[Rd_{red}]} = \frac{k_{red}}{[Rd_{ox}]} \quad (2)$$

where $\upsilon(\nu)$ is the absorption, C a scaling factor, $T_{2ox/red}$ are the intrinsic transverse relaxation times, k_{ox} and k_{red} are the pseudo-first-order rate constants of the reduction and oxidation of the protein, respectively, and k_{ese} is the second-order ese rate constant.

Any accurate determination of the parameters involved in these equations requires precise simulation of the experimental spectra. This has been carried out by a least-squares minimization between the calculated and experimental spectra using the complete band shape (CBS) method (*34*). In the latter, the scaling factor C allows to adjust the total concentration of the protein. If the chemical shift difference, $\delta\nu$, in the absence of exchange and the transverse relaxation times, $T_{2ox/red}$, can be separately determined with fully oxidized and fully reduced samples, the adjustable parameters left are the molar fractions of each species, p_{ox} and p_{red}, and the pseudo-first-order rate constant, k'. Two minimizations have been implemented. One uses a nonlinear fitting procedure of the digitized experimental spectra based on the Marquardt−Levenberg algorithm. The other is an iterative routine first determining the direction of convergence and then optimizing either one parameter at a time, as applied to all parameters in turn, or two parameters (e.g. ν_{ox}, ν_{red}) together in a concerted way. The latter procedure permits a better estimate of the drift toward a minimum of the highly correlated sought parameters. The programs used in these procedures were written in TurboPascal (v.6) and implemented on personal computers.

Application to Rubredoxin. To obtain reliable determinations of the parameters, it is important to record the different NMR spectra under conditions as identical as possible for all samples. Toward this aim, the amplification gain, the spectral width, and the position of the sample in the probe were kept constant. Spectra were referenced to the transmitter offset (at −577 Hz on the 400 MHz instrument and at −162 Hz on the 500 MHz one) and were recorded with 16K complex points (32K at 500 MHz). Gaussian apodization, without line broadening of the studied signals, was applied to the FID before Fourier transformation.

The NMR lines assigned to the δCH_3 protons of Ile33 were first simulated in fully oxidized and fully reduced spectra of the protein. This gave $\delta\nu$, T_{2ox}, and T_{2red} [$T_2 = 1/(\pi\Gamma)$, where Γ is the width at half-height] for all experimental conditions (temperature, ionic strength, pH). It should be noticed that the positions of the NMR lines ($\delta\nu$ around 50 Hz) vary slightly (less than 2 Hz) as a function of ionic strength over the 0−0.1 M range and sharply (more than 10 Hz) in the 13−38 °C temperature range. These parameters were then used to simulate normalized experimental spectra of semireduced samples. Because of the many contributors to the uncertainties in these measurements (protein concentration, ionic strength, NMR measurements, and fitting procedure to name but a few), it is unrealistic to attempt a rigorous error calculation on the resulting parameters. However, because of the smooth variations with ionic strength of the determined values despite the large changes in the shape of the spectra, a reasonable estimate of the relative error appears to be around 30%.

Calculations of Electrostatic Interactions and Ionic Strength Independent Rate Constants

The k_{ese} data obtained from NMR experiments were fitted to the "parallel plate" electrostatic model for bimolecular interactions (*35*). In this model, the rate constant measured at ionic strength I is given by

$$\ln k(I) = \ln k_\infty - V_{ii}X(I) - V_{id}Y(I)X(I) - V_{dd}Y(I)^2Z(I) \quad (3a)$$

in which $X(I)$, $Y(I)$, and $Z(I)$ are functions of the ionic strength whose expressions can be found in the original reference (*35*) and

$$V_{ii} = \alpha Z_1 Z_2 r_{12}/D_e\rho^2 \quad (3b)$$

$$V_{id} = \alpha[(Z_1\mu^\circ_2 \cos\theta_2)/(r_{12} + R_2)^2 + (Z_2\mu^\circ_1 \cos\theta_1)/(r_{12} + R_1)^2]/D_{id}$$

$$V_{dd} = \alpha\mu^\circ_1\mu^\circ_2 \cos\theta_{12}/(r_{12} + R_1 + R_2)^3 D_{dd}$$

$$\alpha = e^2/2\pi k_B T$$

$$\mu^\circ = \mu/D_i$$

where k_B is the Boltzmann constant, Z_i are the charges of the interacting sites, r_{12} the distance separating them, ρ their radius, μ the dipole moments of the molecules, R their radii, and the angles θ are defined by the relative orientations of the dipoles of the two molecules or of each molecule versus the direction linking the two active centers. D_e and D_i are the effective dielectric constant at the site of interaction and the internal dielectric constant, respectively. D_{id} and D_{dd} are functions of D_e and D_i (*35*).

In the "parallel plate" model the total electrostatic energy is $V_{tot} = k_B T(V_{ii} + V_{id} + V_{dd})$.

RESULTS

The coordinating sequence motif found in rubredoxins is $CX_1X_2CGX_3$ where X_2 and X_3 generally bear aliphatic side chains. The motif occurs twice in the sequence to provide the four cysteine ligands to the iron. The present studies focus on the N-terminal segment of *C. pasteurianum* rubredoxin in which X_2 is V8 and X_3 is Y11: V8 was replaced by E, G10 by A and E, and Y11 by F, S, C, D, H, and N. All of these molecular variants were purified to homogeneity and displayed similar electronic absorption spectra, except for a slight shift of the 750 nm band to 757 nm in the case of G10A and G10E, as already reported for the former (*24*). These data indicate that the coordination of the ferric ion is the same in all molecular variants. The lack of gross structural change upon these subtitutions was confirmed by the similar NMR patterns exhibited by all reduced and oxidized proteins (see below).

Reduction Potential Measurements

Representative potentiometric titrations carried out at pH 7 are shown in Figure 1. The data could be fitted to the Nernst equation with $n = 1$ as expected and gave the values of the reduction potentials reported in Table 2. These values vary by less than 20 mV, i.e. within the accuracy limits of these measurements, when the ionic strength is changed over the 0.02−0.5 M range, in contrast with the strong dependence exhibited by the ese rate constant (*29*, see below). All substitutions introduced into the protein do induce shifts of the reduction potential. The measured shifts are less than those generally observed upon substitution of one ligand in rubredoxin (*13*) and [2Fe-2S] proteins (*36, 37*) but they are similar to, or larger than, those observed when other residues close to Fe-S active sites are modified (*26, 38*−*42*).

Since values between −55 and −77 mV have already been reported for native *C. pasteurianum* rubredoxin using different methods and conditions (*24, 36, 43, 44*), the potentiometric measurements were checked by square-wave voltammetry (Figure 2, Table 2).

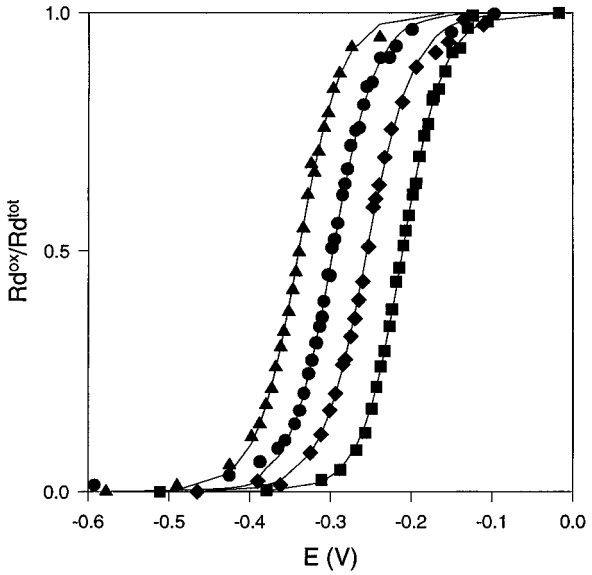

FIGURE 1: Potentiometric titrations of rubredoxin variants. The molar fraction of oxidized rubredoxin is plotted as a function of the potential (in volts) measured *vs* the Ag/AgCl reference electrode. Circles, native rubredoxin; triangles, G10E; diamonds, V8E; squares, Y11N. The solid lines are the results of fitting the data to the Nernst equation.

Table 2: Reduction Potentials of *C. pasteurianum* Rubredoxin and Variants[a]

rubredoxin	*E* (mV *vs* NHE)	rubredoxin	*E* (mV *vs* NHE)
native	−95; −95	G10A	−120; −104
V8E	−70; −75	G10E	−138; −117
Y11F	−82 (P)	Y11H	−55; −68
Y11D	−58; −54	Y11S	−37; −32
Y11C	−56; −51	Y11N	−18; −22

[a] Data were obtained by potentiometry (P, left value) and by square wave voltammetry (SWV, right value).

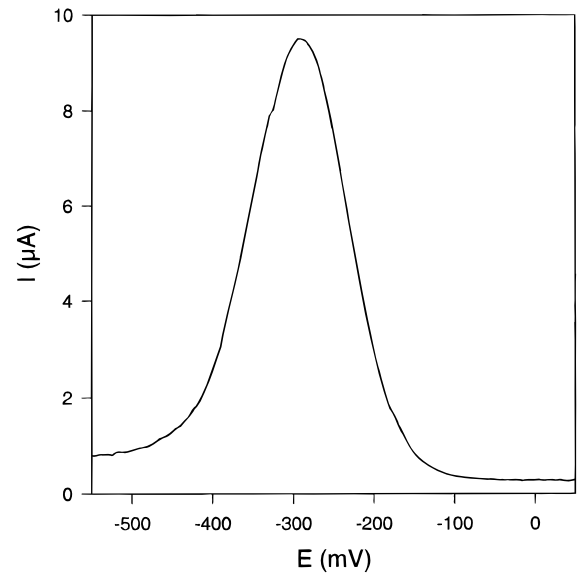

FIGURE 2: Square wave voltammogram of *C. pasteurianum* rubredoxin. Data recorded at the planar glassy carbon electrode in 5 mM potassium phosphate buffer with ca. 6 mM neomycine. The cathodic current was recorded by applying a step potential of 5 mV, a pulse potential of 50 mV, and a frequency of 5 Hz.

It has already been reported (*27, 44, 24*) that reaction of rubredoxin with carbon electrodes required the use of promoters, such as multivalent cations, to overcome the

Table 3: Self-Exchange Rate Constants of *C. pasteurianum* Rubredoxin and Variants[a]

rubredoxin	k_{ese} (M^{-1} s^{-1})	rubredoxin	k_{ese} (M^{-1} s^{-1})
native	3.1×10^5 [b]	V8E	$<3 \times 10^3$
Y11D	2.6×10^5	G10A	2.4×10^5
Y11N	2.2×10^5	G10E	2.2×10^4

[a] Data obtained at 30 °C in 50 mM phosphate buffer, pH 7.0. [b] Value measured at 33 °C.

strong electrostatic repulsion between the negatively charged carbon and protein surfaces. Here, neomycine, a polycationic aminoglycoside, has been used for this purpose. The electrochemical response of rubredoxin is reversible under the conditions of Figure 2. The cathodic and anodic waves are equivalent with a peak width of 126 ± 2 mV. No significant differences in the electrochemical behaviour of the protein have been found by changing the ionic strength of the solution. This shows that the heterogeneous electron transfer rate between rubredoxin and the electrode is ionic strength independent, in contrast with what has been found for the ese rate constant in solution (*29*). Such apparent discrepancy may be explained by the role of neomycin which helps to shield repulsive charges suspected to slow the ese rate (*29*) and significantly contributes to increase the ionic strength on the electrode layer.

The values of reduction potentials measured by SWV for the molecular variants of rubredoxin agree with those measured by potentiometry (Table 2). It can then be safely concluded that the changes introduced into *C. pasteurianum* rubredoxin do affect the value of the reduction potential.

Electron Self-Exchange Rates

The reduction potential is a measure of the ease with which an electron can be added to, or removed from, the protein active site. Complementary information can be obtained from the value of the ese rate constant determined in a mixture of oxidized and reduced protein. An NMR method previously implemented for rubredoxin (*29*) has been improved herein.

The raw values of the ese rate constants determined for a series of *C. pasteurianum* rubredoxin variants are given in Table 3. It has been checked that these values obey eq 2 for the protein concentrations reported. This is not necessarily true for higher protein concentrations (above ca. 2 mM in the case of native rubredoxin) for which other interactions may occur, as already noticed with other metalloproteins (*45*). Large differences in the values of k_{ese} of up to 2 orders of magnitude (Table 3) can be observed among the rubredoxin variants studied. Significantly enough, those molecular forms bearing a charged residue in position 8 or 10, instead of the aliphatic valine and glycine, respectively, exhibit the slowest rates. Thus the changes in k_{ese} are restricted to V8E and G10E (Table 3) whereas shifts of the reduction potential are measured for all molecular forms investigated (Table 2).

The experimental values of the ese rate constant depend on two main factors, one being the molecular recognition between interacting molecules, and the other the electron transfer reaction in the competent bimolecular complex formed (*1*). To discriminate between them, measurements were carried out at different ionic strengths for selected molecular forms. Also the temperature was varied in the 13−38 °C range at two different pH values of the solution, 7.0 and 5.5.

As already noticed with native rubredoxin over a very narrow ionic strength range (*29*), k_{ese} as measured in the present work generally increases with increasing ionic strength as expected for the reaction between molecules bearing the same charge. However, these data could not be satisfactorily fitted with any of the ionic strength dependencies expected from the electrostatic interactions (*46*) between two molecules bearing the net charges of oxidized and reduced rubredoxin over the range accessible in the present experiments (not shown). Also, the data recorded for the G10E variant at pH 5.5 exhibit a *decrease* of k_{ese} with increasing ionic strength (Figure 3). The latter observation may be explained by a change of the interacting site between pH 7.0 and 5.5. This occurrence would imply that the reduced and oxidized proteins bear opposite effective charges at pH 5.5; although this possibility cannot be ruled out, we consider it unlikely because (i) a single unit charge, as compared to the ca. −10 net charge of the molecule, is exchanged in the reaction, and (ii) all positively charged side chains of rubredoxin being remote from the metal atom (*20, 21*), their involvement at the interacting site should strongly decrease the virtual rate constant calculated at infinite ionic strength at pH 5.5 when compared to pH 7.0. From this type of calculation, a difference of less than 10-fold has been found (not shown) which does not strongly support this explanation.

An alternative interpretation can be based on the involvement of dipolar terms (*47*). Indeed, the values calculated for the dipolar moments of the molecules under consideration (Table 4) may not be negligible in all cases in comparison with the contribution of the individual charges (see below).

The relevant equations to interpret such data have been derived from theoretical model molecules (*35, 46*). One of these models (*46*) considers the total charge of the reactants as homogeneously distributed over the surface without preferential orientations resulting from discrete monopole−monopole interactions. The crystal structure of rubredoxin (*21*) clearly suggests that the protein is unlikely to obey this property because of its highly asymmetric electrostatic potential and we have therefore favored a model in which only the parameters (charge and dipole) of the interacting site(s) are included in the calculations (*35*). It should be noted at the onset of this analysis that all these models contain many parameters and do not afford unique solutions, especially in the cases of monotonous dependencies of k_{ese} as a function of ionic strength (*35*). Nevertheless, the combined observations of disagreement between our data and rate laws derived for electrostatic interactions between small ions (*46*) on the one hand and of the lack of evidence sustaining alternative interacting sites (see above) on the other hand do indicate that *both* monopolar and dipolar terms have to be considered. This has been done by varying the terms relative to all monopole−monopole, monopole−dipole, and dipole−dipole interactions (V_{ii}, V_{id}, and V_{dd}, respectively) over wide ranges, for different values of the radius (ρ) of the interacting site. Representative fits are shown in Figure 3, and the derived parameters are shown in Table 4.

In all these calculations, a radius of about 6 Å of the site of interaction has been found to afford the lowest standard deviation. This value seems reasonable in view of the size of rubredoxin. A common trend of all calculations

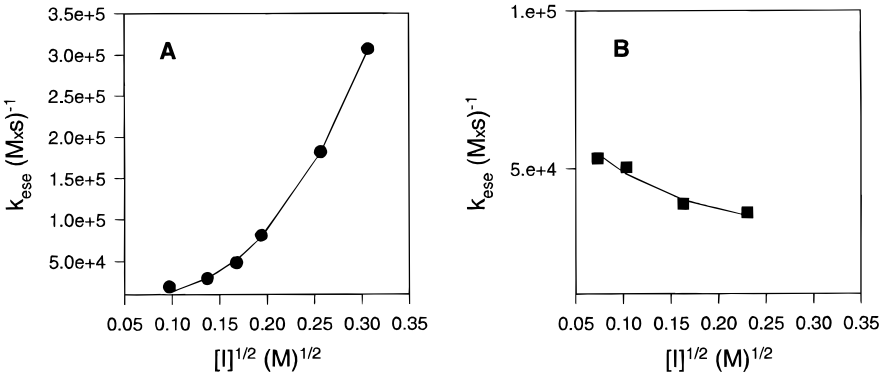

FIGURE 3: Ionic strength dependence of k_{ese}. (A) Native rubredoxin (circles) at 33 °C and pH 7.0. (B) G10E (squares) at 35 °C and pH 5.5. The lines correspond to the fits obtained by applying the parallel plate model, equation 3a.

Table 4: Electrostatic Interaction Parameters Deduced from the "Parallel Plate" Model Fit to k_{ese}[a]

protein	pH	k_∞ (M^{-1} s^{-1})[b]	V_{ii}	$\|Z\|$[c]	V_{id}	V_{dd}	μ[d]
native	7	4.2×10^6 [e]	5.5	2.6	2.5	0.5	28
	5.5	1.6×10^6	4	2.2	1.5	0	
Y11D	7	3.1×10^6	3.5	2.0	1	0.5	57
G10E	7	0.44×10^6	6.5	2.8	1	0.1	85
	5.5	0.03×10^6	3	1.9	−4	0	
V8E	7	0.27×10^6	9	3.3	2	0.2	89
	5.5	0.19×10^6	5	2.5	0	0	

[a] All values were obtained with a radius of the interaction domain set at 6 Å, which gives the lowest standard deviation. The *V* parameters are average values obtained at different temperatures. [b] At 30 °C. [c] Effective charge of the interacting site calculated from eq 3b, assuming $r_{12} = 3.5$ Å and $D_e = 15$. Since the effective charge increase resulting from reduction of the protein at the interacting site defined by the model is not known, it has been taken as zero, i.e., Z_1Z_2 was taken as Z^2. [d] Absolute value of the dipole moment in debye, calculated on the minimized structure of rubredoxin and on the structures obtained by successively substituting the side chains of V8, G10, and Y11. [e] Value at 33 °C.

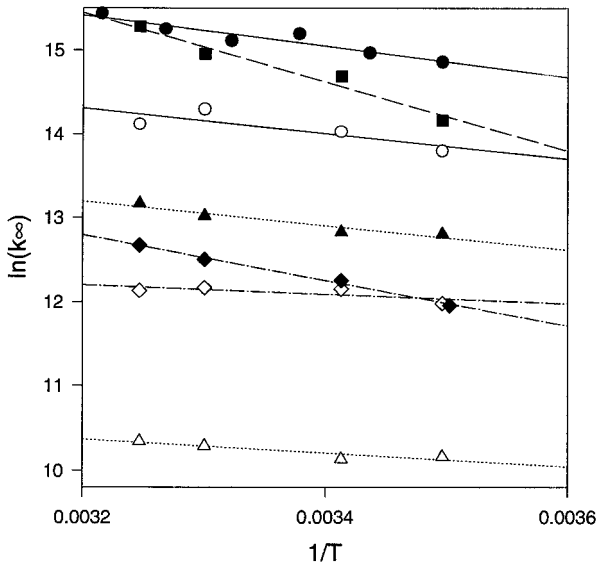

FIGURE 4: Temperature dependence of the electron self-exchange rate constant at infinite ionic strength. The values derived from the observed rates according to eq 3a are plotted according to eq 5. Filled symbols, data at pH 7.0; open symbols, data at pH 5.5. Circles, native rubredoxin; squares, Y11D; triangles, G10E; diamonds, V8E. The lines are linear regressions drawn through the data points.

is the weak relative contribution of the dipole−dipole interactions, as expected from data generally obtained at low ionic strength as investigated herein (*46*). Lowering the pH of the solution results in decreased values of the parameter associated with monopole−monopole interactions (V_{ii}). This is also in line with the shielding of dominating negative charges of rubredoxin occurring upon increasing the proton concentration.

The comparison of the different molecular forms investigated reveals significant differences induced by the amino acid substitutions on V8, G10, and Y11. The parameters relative both to the electrostatic interactions between molecules (V_{ii}, V_{id}, and V_{dd}) and to the electron transfer step (k_∞) experience changes in the different variants. At the level of accuracy attained in these experiments, the expected temperature dependence of the electrostatic terms cannot be precisely measured and it has been neglected as a result of the very small variations exhibited by the fits. In contrast, k_∞ displays a strong temperature dependence that varies significantly with the molecular form considered (Figure 4). All of these observations indicate that the electron transfer complexes are strongly perturbed by the modifications, and their consequences are further analyzed below.

DISCUSSION

The changes introduced in the amino acid sequence of *C. pasteurianum* rubredoxin have not led to large structural perturbations of this simple protein. This is borne out by several pieces of evidence, such as the similar chromatographic behavior, UV−visible, NMR, or EPR spectra of all purified proteins. These observations then allow us to specifically probe the role of the modified residues in modulating the redox and electron transfer properties of the protein. The variations of the reduction potential and of the ese rate constant do not follow the same trends for the series of substitutions investigated. They will therefore be examined in turn.

Reduction Potential Values

On the basis of measurements previously carried out for a series of modified *C. pasteurianum* rubredoxins (*38*), it was suggested that the increased or decreased accessibility of the solvent (water) to the active site could be a dominant factor in increasing or decreasing, respectively, its reduction potential. The data obtained herein on the V8 and G10 variants, as well as elsewhere for other G10 derivatives (*24*), may be interpreted along the same lines. They also confirm the relatively minor contribution of the presence of a charge on these side chains to the value of the reduction potential

Table 5: Water Molecules Neighboring the Active Site During 100 ps Simulations

protein	native	Y11N	V8E	G10E
average no. of water molecules at less than 7 Å from the iron atom	6.9	4.2	5.9	7.1
closest distance between water and iron (Å)	4	5.8	5.3	3.9

(*48*). The molecular dynamics simulations carried out in the present work give average distances between the Cδ of E8 or E10 and the iron atom at 7.2 and 9.7 Å, respectively.

However, our molecular dynamics calculations do not conclusively sustain the interpretation of the reduction potential shifts based on the accessibility of the active site atoms in these mutagenized forms. As an example, the average number of water molecules approaching the iron atom at less than 7 Å and their closest distance over the 100 ps simulations have been calculated (Table 5). It is of note that this ranking is exactly the opposite of that predicted by simple considerations of the bulkiness of the replaced side chains. Also, a water molecule has been found to come near the active site between one side of the FeS_4 unit and the Y11 ring in native and G10E but not in V8E and Y11N. Clearly, more sophisticated descriptions of the interactions between the metal center and its environment (protein and solvent) are needed to fully evaluate the consequences of these substitutions on the value of the reduction potential (*48*, *49*).

Even more challenging are the results obtained with the Y11 variants. The presence of a six-membered aromatic ring (Y, F) affords the most negative values. Positive shifts of at least 30 mV are associated with the replacement by polar (C, H, S, N) or charged (D) residues (Table 2). No straightforward correlations with either the bulkiness of the side chain or its charge are apparent, although in the latter case a distance of about 5.2 Å can be estimated between the iron atom and the Cγ of D11.

Some hints about a possible interpretation of these results arise from the molecular dynamics studies of the Y11N form showing the largest increase in reduction potential compared to the native protein (Table 2). The main outcomes of such simulations are that, on the one hand, the two external $CX_1X_2CGX_3$ β-turns more efficiently shield the metal from access of the solvent (Table 5) and, on the other hand, the removal of the Y11 ring perturbs the core of aromatic residues, mainly F49 close to C6, and F30 to a lesser extent. In this case again a lower number of surrounding water molecules seems to correlate with a less negative value of the reduction potential (Table 5). However, even more important might be the changes introduced by the removal of the aromatic ring in position 11 on the electronic structure of the active site. Indeed, it has been calculated that the bonding interactions between the sulfurs and iron in $[Fe(S\text{-}(2\text{-}(Ph)C_6H_4))_4]^{-/2-}$ model compounds are highly sensitive to the orientation of the thiol ligands (*50*). The substitution of Y11 may slightly move at least some of the ligands in Y11X. In addition, any further electronic effect contributed by surrounding delocalized systems, such as aromatic rings, may interfere with these bonding interactions and shift the value of the reduction potential. Even though rubredoxin is a simple metalloprotein, many contributing factors tune the value of the reduction potential, and only when a full set of completely characterized variants is available will their assessment be possible. The data reported herein demonstrate at least that oversimplistic interpretations of the effects of substituted residues should be avoided with rubredoxins as well as with other metalloproteins (*48*).

Electron Self-Exchange Rates

From the large differences in k_{ese} exhibited by some of the modified forms of rubredoxin (Table 3), some insight into the detailed mechanism of ese may be obtained. In the model used to describe these reactions (*35*), the different parameters relevant both to protein recognition and to electron transfer are highly sensitive to the changes introduced into the molecule (Table 4).

The parallel plate model separates the contributions to the observed rate of the electrostatic interactions between proteins and of the electron transfer step (eq 3, Table 4). The latter translates into a virtual rate constant at infinite ionic strength that is related to the activation parameters of the electron transfer reaction. This rate constant is given by (*1*)

$$k_\infty = \kappa(r)\nu \exp(-\Delta G_r^*/RT) \qquad (4)$$

where κ is a transmission coefficient accounting for the electronic coupling between the donor and acceptor at distance r, ν is a frequency whose meaning depends on the adiabatic or nonadiabatic regime of the reaction, and ΔG_r^* is the free energy of activation.

Equation 4 simplifies to

$$k_\infty = \kappa(r)\nu \exp(-\lambda/4RT) \qquad (5)$$

for ese reactions in which λ is the reorganization energy.

From eq 5, the reorganization energy of the studied reactions could be calculated from the plots of ln k_∞ as a function of $1/T$ (Figure 4) if the temperature dependence of $\kappa(r)\nu$ is neglected relative to that of the activation term. We are reluctant to apply this method because it is not clear why such large differences in the slopes of the curves of Figure 4 are observed between point-mutated forms of rubredoxin. Indeed, unexpected results have already been reported in attempts to derive the value of the reorganization energy from temperature studies with other systems (e.g. *51*). It appears that the temperature dependence of electron transfer rate constants may have other underlying mechanisms than that implied by eqs 4 and 5 above (*52*). Defining the electron transfer parameters of the ese reaction of rubredoxin will thus certainly require further experimental data.

Until such additional information is available, it is worth noting that, for any given protein, the slope at pH 5.5 is smaller than that at pH 7. Also, the values of k_∞ are always smaller at pH 5.5 than at pH 7.0, indicating that the transient complexes formed at low pH are less efficient for ese than those arising in neutral pH solutions. More importantly, the values of k_∞ deduced for V8E and G10E are always at least 1 order of magnitude smaller than those of the native form or Y11D (Figure 4). This observation should be taken as strong evidence that the former two molecules cannot build bimolecular complexes as efficient toward electron transfer as the latter.

In addition to the genuine electron transfer step, the values derived from the analysis using the parallel plate model give

some indication on the relative contributions of the electrostatic interactions to the formation of the transient bimolecular complex. Despite the necessary involvement of the dipolar terms (see above), the dipole−dipole interactions are relatively weak and the dipole−monopole contribution is often less than the monopole−monopole one (Table 4).

From the values of V_{ii}, the effective charge at the site of interaction can be estimated from eq 3b, as described in the legend of Table 4. The values obtained between ca. −2 and −3.5 are very approximate, but in any case they are far smaller than the net charges of the molecules (−10 for oxidized native rubredoxin and most other variants, −11 for oxidized Y11D, V8E and G10E). This indicates that the interaction site of rubredoxin does not involve its numerous highly charged residues. The values of the effective charges calculated in our analysis are, perhaps fortuitously, only slightly larger than those calculated from the mere charge of the metal binding site, i.e. −1 for oxidized (Fe^{3+} and 4 Cys), −2 for reduced rubredoxin. The largest values of Z at neutral pH are also found for the V8E and G10E variants, in agreement with the above proposal that these charged residues lie close to, if not at, the site of interaction between rubredoxin molecules.

In contrast to the monopole−monopole term, the monopole−dipole one is highly variable, although generally small. This agrees with the fact that both the value and the orientation of the total dipole of rubredoxin are strongly dependent on the charges introduced in the side chains surrounding the active site. As the dipolar contribution enters V_{id} as $\mu \cos \theta$, where μ is the absolute value of the dipole moment and θ is the angle between the direction of this moment and the line connecting the Fe atoms of the bimolecular complex(es), it is impossible without knowing the geometry of the latter complex(es) to assign the (relatively minor) changes of this parameter to any of these factors (intensity and orientation). In any case, the results of these analyses do point to an interplay between monopolar and dipolar contributions to the electrostatic interactions between rubredoxin molecules, as now generally accepted for many other biomolecules (e.g. *35*, *53*, *54*). In addition, the actual charge contributing to the monopolar repulsion is far smaller than could be expected solely based on the total charge of the molecule and is more in agreement with the charge density suspected to surround the active site only.

CONCLUSIONS

The data for *C. pasteurianum* rubredoxin, obtained as a result of extensive site-directed mutagenesis (*24*, *38*, this work), are starting to reveal the fine molecular details determining the properties of this prototypical electron transfer protein. Concerning the functional properties analyzed herein, neither the value of the reduction potential nor that of the ese rate constant can be easily predicted based on the simple considerations previously put forward (*38*). In particular, the accurate value of k_{ese} provided in this work and its variations as a function of ionic strength or molecular changes do not support the direct overlap of the redox active rubredoxin orbital with that of a redox partner (*55*). The role of the solvent for instance appears to be very important, as already suggested by molecular dynamics simulations of the crystal structure (*56*).

Clearly additional structural data on both redox levels of the protein and on the nature of the bimolecular complex(es) implicated in electron self-exchange would be needed to validate the interpretation proposed in the present work. The atomic structure of this protein, either reduced or oxidized, can be obtained with exceptionally high accuracy (better than 1 Å resolution),[2] and electron transfer complexes can now be realistically simulated (*57*, *58*). It may then be expected that rubredoxin will provide an unprecedented insight into the molecular details of an electron transfer reaction involving a protein, a matter of current interest and debate for many other electron transfer proteins (e.g., *45*−*47*, *51*−*54*). Such future studies will have to integrate the involvement of residues 8 and 10 at the site of interaction between molecules demonstrated herein.

ACKNOWLEDGMENT

Professor Gordon Tollin is thanked for providing the computer program used to fit the data to the parallel plate model and for his challenging comments. We are grateful to Dr. Jacques Meyer for carefully reading the manuscript.

REFERENCES

1. Marcus, R. A., and Sutin, N. (1985) *Biochim. Biophys. Acta 811*, 265−322.
2. Moser, C. C., Page, C. C., Farid, R., and Dutton, P. L. (1995) *J. Bioenerg. Biomembr. 27*, 263−274.
3. Gray, H. B., and Winkler, J. R. (1996) *Annu. Rev. Biochem. 65*, 537−561.
4. Raphael, A. L., and Gray H. B. (1991) *J. Am. Chem. Soc. 113*, 1038−1040.
5. Bertrand, P., Mbarki, O., Asso, M., Blanchard, L., Guerlesquin, F., and Tegoni, M. (1995) *Biochemistry 34*, 11071−11079.
6. Kassner, R. J. (1972) *Proc. Natl. Acad. Sci. U.S.A. 69*, 2263−2267.
7. Kassner, R. J. (1973) *J. Am. Chem. Soc. 95*, 2674−2677.
8. Adman, E., Watenpaugh, K. D., and Jensen, L. H. (1975) *Proc. Natl. Acad. Sci. U.S.A. 72*, 4854−4858.
9. Rodgers, K. K., and Sligar, S. G. (1991) *J. Am. Chem. Soc. 113*, 9419−9421.
10. Warshel, A., and Åqvist, J. (1991) *Annu. Rev. Biophys. Biophys. Chem. 20*, 267−298.
11. Sharp, K. A., and Honig, B. (1990) *Annu. Rev. Biophys. Biophys. Chem. 19*, 301−332.
12. Davis, M. E., and McCammon, J. A. (1990) *Chem. Rev. 90*, 509−521.
13. Meyer, J., Gaillard, J., and Lutz, M. (1995) *Biochem. Biophys. Res. Commun. 212*, 827−833.
14. Iwata, S., Saynovits, M., Link, T. A., and Michel, H. (1996) *Structure 4*, 567−579.
15. Fee, J. A., Mayhew, S. G., and Palmer, G. (1971) *Biochim. Biophys. Acta 245*, 196−200.
16. Moulis, J.-M., Lutz, M., Gaillard, J., and Noodleman, L. (1988) *Biochemistry 27*, 8712−8719.
17. Moulis, J.-M., and Meyer, J. (1982) *Biochemistry 21*, 4762−4771.
18. Calzolai, L., Gorst, C. M., Zhao, Z.-H., Teng, Q., Adams, M. W. W., and LaMar, G. N. (1995) *Biochemistry 34*, 11373−11384.
19. Babini, E., Bertini, I., Borsari, M., Capozzi, F., Dikiy, A., Eltis, L. D., and Luchinat, C. (1996) *J. Am. Chem. Soc. 118*, 75−80.
20. Dauter, Z., Sieker, L. C., and Wilson, K. S. (1992) *Acta Crystallogr. B 48*, 42−59.
21. Dauter, Z., Wilson, K. S., Sieker, L. C., Moulis, J.-M., and Meyer, J. (1996) *Proc. Natl. Acad. Sci. U.S.A. 93*, 8836−8840.
22. Moulis, J.-M., Davasse, V., and DeJésus, F. (1994) *Biometals 7*, 272−278.
23. Mathieu, I., Meyer, J., and Moulis, J.-M. (1992) *Biochem. J. 285*, 255−262.

24. Ayhan, M., Xiao, Z. G., Lavery, M. J., Hamer, A. M., Nugent, K. W., Scrofani, S. D. B., Guss, M., and Wedd, A. G. (1996) *Inorg. Chem. 35*, 5902−5911.
25. Tabor, S. (1990) in *Current Protocols in Molecular Biology* (Ausubel, F. A., Brent, R., Kingston, R. E., Moore, D. D., Seidman, J. G., Smith, J. A., and Struhl, K., Eds.) pp 16.2.1−16.2.11, Greene Publishing and Wiley-Interscience, New York.
26. Quinkal, I., Davasse, V., Gaillard, J., and Moulis, J.-M. (1994) *Protein Eng. 7*, 681−687.
27. Hagen, W. R. (1989) *Eur. J. Biochem. 182*, 523−530.
28. Haladjian, J., Bianco, P., Nunzi, F., and Bruschi, M. (1994) *Anal. Chim. Acta 289*, 15−20.
29. Gaillard, J., Zhuang-Jackson, H., and Moulis, J.-M. (1996) *Eur. J. Biochem. 238*, 346−349.
30. Bloch, F. (1946) *Phys. Rev. 70*, 460−474.
31. Gutowsky, H. S., and Holm, C. H. (1956) *J. Chem. Phys. 25*, 1228−1234.
32. McConnell, H. M. (1958) *J. Chem. Phys. 28*, 430−431.
33. Rogers, M. T., and Woodbrey, J. C. (1962) *J. Chem. Phys. 25*, 540−546.
34. Sandström, J. (1982) *Dynamic NMR Spectroscopy*, Academic Press, London.
35. Watkins, J. A., Cusanovich, M. A., Meyer, T. E., and Tollin, G. (1994) *Protein Sci. 3*, 2104−2114.
36. Cheng, H., Xia, B., Reed, G. H., and Markley, J. L. (1994) *Biochemistry 33*, 3155−3164.
37. Moulis, J.-M., Davasse, V., Golinelli, M.-P., Meyer, J., and Quinkal, I. (1996*) J. Bioinorg. Chem. 1*, 2−14.
38. Zeng, Q., Smith, E. T., Kurtz, D. M., Jr., and Scott, R. A. (1996) *Inorg. Chim. Acta 242*, 245−251.
39. Golinelli, M.-P., Akin, L. A., Crouse, B. R., Johnson, M. K., and Meyer, J. (1996) *Biochemistry 35*, 8995−9002.
40. Uhlmann, H., and Bernhardt, R. (1995) *J. Biol. Chem. 270*, 29959−29966.
41. Vidakovic, M., Fraczkiewicz, G., Dave, B. C., Czernuszewicz, R. S., and Germanas, J. P. (1995) *Biochemistry 34*, 13906−13913.
42. Hidalgo, E., Ding, H., and Demple, B. (1997) *Cell 88*, 121−129.
43. Lovenberg, W., and Sobel, B. E. (1965) *Proc. Natl. Acad. Sci. U.S.A. 54*, 193−199.
44. Armstrong, F. A., Cox, P. A., Hill, H. A. O., Lowe, V. J., and Oliver, B. N. (1987*) J. Electroanal. Chem. 217*, 331−366.
45. Dixon, D. W., Hong, X., and Woehler, S. E. (1989) *Biophys. J. 56*, 339−351.
46. Van Leeuwen, J. W. (1983) *Biochim. Biophys. Acta 743*, 408−421.
47. Koppenol, W. H. (1980) *Biophys. J. 29*, 493−508.
48. Warshel, A., Papazyan, A., and Muegge, I. (1997*) J. Bioinorg. Chem. 2*, 143−152.
49. Stephens, P. J., Jollie, D. R., and Warshel, A. (1996) *Chem. Rev. 96*, 2491−2513.
50. Gebhard, M. S., Koch, S. A., Millar, M., Devlin, F. J., Stephens, P. J., and Solomon, E. I. (1991) *J. Am. Chem. Soc. 113*, 1640−1649.
51. Kyritsis, P., Huber, J. G., Quinkal, I., Gaillard, J., and Moulis, J.-M. (1997) *Biochemistry 36*, 7839−7846.
52. Barbara, P. F., Meyer, T. J., and Ratner, M. A. (1996) *J. Phys. Chem. 100*, 13148−13168.
53. Dixon, D. W., Hong, X., Woehler, S. E., Mauk, A. G., and Sishta, B. P. (1990) *J. Am. Chem. Soc. 112*, 1082−1088.
54. Davidson, V. L., and Jones, L. H. (1995) *Biochemistry 34*, 1238−1243.
55. Holm, R. H., Kennepohl, P., and Solomon, E. I. (1996) *Chem. Rev. 96*, 2239−2314.
56. Yelle, R. B., Park, N.-S., and Ichiye, T. (1995) *Proteins 22*, 154−167.
57. Andrew, S. M., Thomasson, K. A., and Northrup, S. H. (1993) *J. Am. Chem. Soc. 115*, 5516−5521.
58. Ullmann, G. M., Knapp, E.-W., and Kostic, N. M. (1997) *J. Am. Chem. Soc. 119*, 42−52.

BI971636E